

Environmental dependence of polycyclic aromatic hydrocarbon emission at $z \sim 0.8$

Investigation by observing the RX J0152.7-1357 with AKARI

Kazumi Murata¹, Yusei Koyama^{1,2}, Masayuki Tanaka², Hideo Matsuhara¹, and Tadayuki Kodama²

¹ Institute of Space and Astronautical Science, Japan Aerospace Exploration Agency, Sagami-hara, Kanagawa 229-8510, Japan
e-mail: murata@ir.isas.jaxa.jp

² National Astronomical Observatory of Japan, Osawa 2-21-1, Mitaka, Tokyo 181-8588, Japan

Received April 1, 2015; accepted June 29, 2015

ABSTRACT

We study the environmental dependence of the strength of polycyclic aromatic hydrocarbon (PAH) emission by AKARI observations of RX J0152.7-1357, a galaxy cluster at $z=0.84$. PAH emission reflects the physical conditions of galaxies and dominates $8 \mu\text{m}$ luminosity (L_8), which can directly be measured with the L15 band of AKARI. L_8 to infrared luminosity (LIR) ratio is used as a tracer of the PAH strength. Both photometric and spectroscopic redshifts are applied to identify the cluster members. The L15-band-detected galaxies tend to reside in the outskirts of the cluster and have optically green colour, $R - z' \sim 1.2$. We find no clear difference of the L_8/LIR behaviour of galaxies in field and cluster environment. The L_8/LIR of cluster galaxies decreases with specific-star-formation rate divided by that of main-sequence galaxies, and with LIR, consistent with the results for field galaxies. The relation between L_8/LIR and LIR is between those at $z = 0$ and $z = 2$ in the literature. Our data also shows that starburst galaxies, which have lower L_8/LIR than main-sequence, are located only in the outskirts of the cluster. All these findings extend previous studies, indicating that environment affects only the fraction of galaxy types and does not affect the L_8/LIR behaviour of star-forming galaxies.

Key words. – infrared: galaxies – galaxies: starburst – galaxies: clusters: individual (RX J0152.7-1357)

1. Introduction

Galaxy formation and evolution are highly affected by its environment. In the local Universe, galaxies in clusters tend to be red, early type (Dressler 1980) and show lower star-forming activities. This star formation - density relation can also be seen in the distant universe (Quadri et al. 2012), while some studies suggest that the relation is reversed at $z \geq 1$ (Elbaz et al. 2007; Cooper et al. 2008). Although star formation - density relation at higher redshift is still under debate, it is clear that the environment must play an important role in galaxy formation.

Recent studies suggest that the environment affects only the fraction of galaxy types, and star-forming galaxies in different environment have similar properties (Patel et al. 2009a; Muzzin et al. 2012; Koyama et al. 2013, 2014). Patel et al. (2009a) suggest that lower star formation rate (SFR) of galaxies in higher density may reflect the lower fraction of star forming galaxies, rather than a decrease of SFRs. Koyama et al. (2013) discusses that SFR - stellar mass (M_*) relation of $H\alpha$ selected galaxies is independent of the environment since $z \sim 2$. On the other hand, they also show that the dust attenuation and the median SFR of $H\alpha$ emitters are higher in higher density environment at $z = 0.4$, which can be seen only with infrared data. Some studies reported that dusty star-forming galaxies reside in groups (Koyama et al. 2008, 2011; Tran et al. 2009). These studies imply that dust has important roles in understanding the environmental effects on galaxy formation.

Polycyclic aromatic hydrocarbon (PAH) is dust showing prominent features at mid-infrared (MIR). They are excited by UV light from young stars and emit the energy at 3.3, 6.2, 7.7,

8.6 and $11.3 \mu\text{m}$ (Draine & Li 2007). Among the PAH bands, 7.7 and $8.6 \mu\text{m}$ features dominate $8 \mu\text{m}$ luminosity (L_8) even in broad band filters, so that L_8 is used as a PAH luminosity tracer. Due to its energy sources, the PAH emission has been thought to correlate with the infrared luminosity (LIR), which is correlated with SFR. Recent works suggest that high specific SFR (sSFR) galaxies tend to show weak PAH emission compared with main-sequence galaxies (Elbaz et al. 2011; Nordon et al. 2012; Murata et al. 2014). The main causes of the PAH weakness is thought to be destruction of PAHs or a lack of UV photon that excites the PAHs. These studies indicate that the PAH emission traces the physical conditions of the interstellar matter rather than the SFR. On the other hand, the relation between infrared luminosity and PAH emission evolve with redshift (Takagi et al. 2010; Nordon et al. 2012). It suggests that the physical conditions of galaxies with given infrared luminosity is different at different redshift. Hence, if the cluster environment affects the galaxy properties, the relation between infrared luminosity and PAH emission may be different.

However, the behaviour of the PAH emission in cluster environments has not yet been studied well. This is mainly due to sparse filter sampling at $8\text{--}24 \mu\text{m}$ in the *Spitzer* space telescope (Werner et al. 2004), where $7.7 \mu\text{m}$ PAH emission of galaxies at $z < 2$ is redshifted. In contrast, Japanese AKARI satellite (Murakami et al. 2007) has continuous wavelength coverage at $2\text{--}24 \mu\text{m}$ with nine photometric bands in the infrared camera (IRC; Onaka et al. 2007). It enables us to measure the PAH emission at $z < 2$.

The galaxy cluster RX 0152.7-1357 (here after RXJ0152) at $z \sim 0.84$ is one of the suitable targets for investigating an

environmental dependence of dust properties. It is one of the most distant clusters discovered by the *ROSAT* deep cluster survey (Rosati et al. 1998). The $z \sim 0.8$ is suitable redshift, at which the rest frame $8 \mu\text{m}$ luminosity can directly be measured with the *AKARI*'s L15 band. This cluster has been studied by many researchers, so that a number of ancillary data is available: spectroscopically confirmed members are provided in Demarco et al. (2005, 2010); Tanaka et al. (2006); Jørgensen et al. (2005). It was observed by MIPS on-board *Spitzer* (Marcillac et al. 2007), by *Chandra* (Martel et al. 2007), by PACS and SPIRE on-board *Herschel* (Lutz et al. 2011; Oliver et al. 2012) and by *Subaru*/Suprime-cam (Kodama et al. 2005). This cluster is known to have at least three X-ray clumps (Girardi et al. 2005; Maughan et al. 2006), where two main clumps are expected to merge (Demarco et al. 2005). In these clump regions, most of galaxies are not star-forming (Homeier et al. 2005; Marcillac et al. 2007), and exhibit early-type morphology (Nantais et al. 2013). It is believed that they have formed the bulk of the stars in a short period burst at earlier epoch (Ferré-Mateu et al. 2014).

By observing the RXJ0152 with AKARI, we investigate the behaviour of the PAH emission of cluster galaxies, and compare it with the results for field galaxies presented in Murata et al. (2014) to complement the known cluster properties and to improve our understanding of environmental impact on galaxy evolution. This work is organised as follows. Data and methods are described in section 2. Section 3 provides our results, and they are discussed and summarised in section 4. Throughout this paper, we adopt a cosmology with $(\Omega_m, \Omega_\Lambda, H_0) = (0.3, 0.7, 70 \text{ km s}^{-1} \text{ Mpc}^{-1})$, so that 1 arcsec corresponds to 7.6 kpc at $z = 0.8$. An initial mass function of Chabrier (2003) is assumed.

2. Data and Methods

In this study, we investigate PAH behaviour of RXJ0152 galaxies and compare it with that of field galaxies studied in Murata et al. (2014). We adopt L8 to L1R ratio as a tracer of PAH strength, and ratio of L1R to M_* as starburst strength, following our previous studies on the AKARI north ecliptic pole deep survey (Matsuhara et al. 2006; Wada et al. 2008; Murata et al. 2013, hereafter NEP-Deep). We derive these quantities using *AKARI*/IRC, *Spitzer*/IRAC and MIPS, *Herschel*/PACS and SPIRE, and *Subaru*/S-cam.

2.1. AKARI/IRC

Twelve *AKARI*/IRC pointed observations were conducted on 2007 July 12–13 using S7 and L15 bands with AOT05 astronomical templates (Onaka et al. 2007). The AOT05 takes ~ 30 sub-images with 16.4 seconds without dithering and filter change to obtain long exposure time. The field of view of the S7 and L15 band images are separated by ~ 20 arcmin. The observations consist of two fields, F1(RA=28.1679, DEC=-13.9683) and F2(RA=28.3029, DEC=-13.9141). The F1 field was observed four times with the L15 band and three times with the S7, while the F2 field was observed twice with the L15 and three times with the S7.

The image reduction was performed on the basis of standard manner. The linearity correction, the dark subtraction, and the flat fielding were done with the *AKARI*/IRC imaging pipeline (version 131202). The other detail reduction was performed in the same way in Murata et al. (2013). The world coordinate system (WCS) information was registered using *Spitzer*/IRAC and

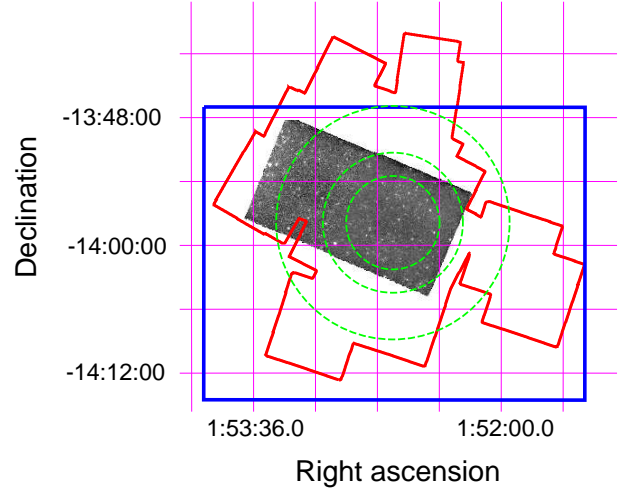


Fig. 1. Mosaicked L15 image ($\sim 10 \times 20 \text{ arcmin}^2$). The blue square and the red line indicate *Subaru*/S-cam and *Spitzer*/MIPS coverages. The green broken circles indicate 2, 3, and 5 Mpc radii from the cluster centre.

MIPS images downloaded from the IRSA web site¹. Bad pixels were removed using the all-dark-frame-stacked images. The sky background was subtracted from each sub-frame using a sky map provided by SExtractor (Bertin & Arnouts 1996). Finally, all images were mosaicked, during which the pixel sizes were reduced to $1 \times 1 \text{ arcsec}^2$ from 2.34×2.34 and $2.51 \times 2.39 \text{ arcsec}^2$ for the S7 and L15 band images, respectively. Figure 1 shows the mosaicked L15 image, which covers a $\sim 10 \times 20 \text{ arcmin}^2$ region. The green broken circles indicates 2, 3, and 5 Mpc from the cluster centre, RA=28.175, DEC=-13.965 (Romer et al. 2000). The L15 image covers the region of $R < 2 \text{ Mpc}$ around the cluster.

Source extraction was performed on the mosaic images using the SExtractor. Sources with five connected pixels having above 1σ from the local background were detected. Although this detection criteria may be too generous, which leads some fake sources, they were removed from the final sample because we use only objects with an optical and MIPS counterpart. The source fluxes were measured with 6 arcsec aperture radius, for which Murata et al. (2013) estimated the photometric calibration. The 5σ detection limits estimated with random sky photometry were 76 and $268 \mu\text{Jy}$ for the S7 and L15 bands, respectively. These values may be overestimated due to residual sky background. The flux errors derived with the sky deviation in the annulus of 20 arcsec with 15 arcsec width were scaled to be consistent with the above detection limits. Although it may lead overestimation, we decided to apply these conservative errors.

2.2. Spitzer/IRAC and MIPS

We retrieved the *Spitzer* data from the IRSA website. All post-basic-calibrated data (PBCD) around the cluster was downloaded for both IRAC and MIPS. Sky background was subtracted from each image using a median filtered image after masking the sources. After the sky subtraction, all images were aligned and combined with median values. The red line in Fig. 1 shows the coverage map of the MIPS image, which covers $R < 3 \text{ Mpc}$ from the cluster centre. The IRAC image also covers $R \lesssim 3 \text{ Mpc}$, although it is not shown in the figure for simplicity.

¹ <http://irsa.ipac.caltech.edu/Missions/spitzer.html>

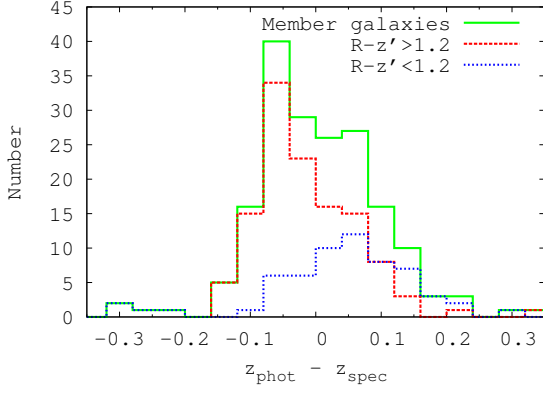


Fig. 2. Distribution of $z_{\text{phot}} - z_{\text{spec}}$ for 186 member galaxies. The red and blue histograms indicate the number of optically red ($R - z' > 1.2$) and blue ($R - z' < 1.2$) galaxies, respectively.

Source extraction was performed using the SExtractor. Sources with five connected pixels above 1σ from the background were extracted. Similar to *AKARI* sources, fake sources were contained, but they can be removed because we use only objects with an optical counterpart. Photometry was simultaneously done for the IRAC 1-4 channels with the dual mode of the SExtractor, where we used the [3.6] band image as the detection image and the aperture radius was set to 6 arcsec. Photometry for the MIPS 24 μm band was done with a 7 arcsec aperture radius and the sky background was estimated from the annulus of 15 arcsec with 5 arcsec width. While the sky background in the IRAC images was subtracted by the SExtractor, we determined the sky background level of MIPS image with an annulus around each source. This is because the MIPS image has some artificial structures and the sky background should be measured from a region near the source position. The flux errors were estimated in the same way as we did for the *AKARI* sources.

2.3. *Herschel*/PACS and SPIRE

Herschel observed the RXJ0152 as PACS evolutionary probe (PEP; Lutz et al. 2011), and the catalogue of 100 and 160 μm bands of the PACS and 250, 350, and 500 μm bands of the SPIRE are available. We downloaded all these catalogues from the CDS². Although it is also observed with SPIRE as *Herschel* multi-tiered extragalactic survey (Oliver et al. 2012), we did not use these data for simplicity.

2.4. *Subaru*/Suprime-Cam

Subaru/S-cam $VRI'z'$ images were obtained in Kodama et al. (2005) and Tanaka et al. (2005). The reduction procedure is described in Kodama et al. (2005). The detection limits of these bands with 2 arcsec aperture were reported as 26.7, 26.5, 26.1, and 25.0, for V , R , i' , and z' bands, respectively. The coverage is shown in Fig. 1 with the blue square. Source extraction was also done using the SExtractor and objects with 5 connected pixels whose values were more than 1.5σ above the background were detected. These detection criteria are the default parameters of the SExtractor. Photometry was performed with the dual mode using the z' band image as the detection image, and *MAG_AUTO* was applied for measuring the total magnitudes.

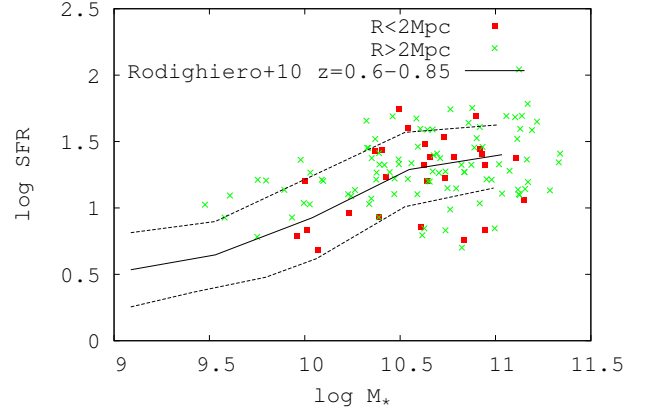


Fig. 3. Star-formation rate versus stellar mass. The red squares and the green crosses indicate galaxies located in $R < 2$ Mpc and $R > 2$ Mpc, respectively. The black solid and broken lines indicate the average and the 1σ range of main-sequence relation for field galaxies at $z = 0.6-0.85$ (Rodighiero et al. 2010).

Because magnitude errors output from the SExtractor is underestimated, we added 0.05 magnitude to the errors, although it is arbitrary.

2.5. Matching the catalogues

To merge the above catalogues, the sources were cross-matched with the nearest neighbour method. *Subaru* sources were matched with *Spitzer*/IRAC sources with a 1 arcsec search radius. IRAC sources were matched with *AKARI*/S7, L15, and MIPS24 sources with 2.5 arcsec radii, respectively, where the size of the 2.5 arcsec search radius is the same as the matching radius used in Murata et al. (2013). Finally, *Herschel*/PACS and SPIRE sources were matched with MIPS24 sources with 5 and 6 arcsec radii, which are the same as in Murata et al. (2014). We used only objects that have both IRAC and *Subaru* photometry to avoid fake sources and to make photometric redshifts reliable. Also, L15-detected objects without MIPS 24 μm photometry, which may be due to matching errors, was not used in this study.

We also matched these sources with spectroscopically confirmed members provided by previous studies (Demarco et al. 2005, 2010; Jørgensen et al. 2005; Blakeslee et al. 2006; Tanaka et al. 2006). All these sources were matched with *Subaru* sources with a 1 arcsec search radius. The redshift of the member galaxies from Blakeslee et al. (2006) were assumed to be $z = 0.84$. Following Patel et al. (2009b), we assumed objects with $z_{\text{spec}} = 0.80-0.87$ are member galaxies. A total of 186 spectroscopically confirmed members were matched with our catalogue, among which 17 objects were detected with both the *AKARI* L15 band and the MIPS24 band. The brightest cluster galaxies defined in Stott et al. (2010) and Lidman et al. (2013) are not detected with the L15 band. We note that 41 member objects were rejected due to a lack of IRAC photometry. We also note that X-ray sources from Martel et al. (2007) are not matched with our catalogue due to blending other sources, although it can visually be confirmed. Hence, we assume that a strong active galactic nucleus is not in our sample.

² <http://cdsweb.u-strasbg.fr/>

2.6. Photometric redshifts

The photometric redshifts were calculated using a publicly available software, LePHARE (Ilbert et al. 2006; Arnouts et al. 2007). It performs a template fitting with the spectral energy distribution (SED) for each object, and calculates photometric redshift as well as physical parameters, with which the minimum χ^2 is provided. We used AVEROIN SED templates (Arnouts et al. 2007) with an interstellar extinction law of SMC following Arnouts et al. (2007). Following Murata et al. (2014), the AVEROIN templates were used only for estimating photometric redshifts because the AVEROIN is suitable for photometric redshift estimation due to small parameter sets. The *Subaru/S-cam* $VRi'z'$ to IRAC [3.6] and [4.5] were fitted with the templates, where [3.6] and [4.5] covers longer wavelength than a stellar bump at $1.6 \mu\text{m}$.

The accuracy of the photometric redshifts was calculated with spectroscopic redshifts. Figure 2 shows the distribution of the difference of photometric and spectroscopic redshifts for the 186 member galaxies. The histograms for blue and red galaxies are also shown for comparison. Although the averages of the $z_{\text{phot}} - z_{\text{spec}}$ for red and blue galaxies have an offset from zero, the average of all sample without outliers is $z_{\text{phot}} - z_{\text{spec}} = -0.0038$. The dependence of the accuracy on optical colours is also reported in Tanaka et al. (2006). Although their sample shows that bluer galaxies have lower photometric redshift, our sample showed an opposite trend. It can be due to the difference of SED templates used in the estimation. The colour dependence of the photometric redshift accuracy affects the fraction of star-forming galaxies, as Tanaka et al. discussed. Nonetheless, this effect should be similar in both the cluster core and the outskirts and our conclusion should not be affected by this effect. The standard deviation is $\sigma_{zp} = 0.080$, which corresponds to $\delta z_{\text{phot}} / (1 + z_{\text{spec}}) = 0.044$. Ten outliers having $z_{\text{phot}} > 3\sigma$ were clipped in the calculation. The z_{phot} average and standard deviation for the member galaxies are $z_{\text{phot}} = 0.843 \pm 0.0825$, and therefore we assumed that objects with $z_{\text{phot}} = 0.76 - 0.925$ are cluster member galaxies. Although a fraction of member galaxies are missed in the criteria, we decided to apply it to avoid an increase of interlopers.

In total, 1922 galaxies were identified as member galaxies, among which 122 have MIPS photometry. Among the total sample, 333 galaxies were located in the $R < 2$ Mpc region, of which 38 objects were detected with the *AKARI* L15 band. We visually checked the SEDs of these MIPS detected sources, and found no galaxies with an unusual SED. In the following, the redshift of cluster members without spectroscopic redshift is set to $z = 0.84$.

2.7. Deriving physical parameters with SED fitting

The main purpose of this paper is to compare the $L8/\text{LIR}$ behaviour of cluster and field galaxies at $z = 0.8$. We derive LIR, M_* , and $L8$ with the LePHARE in the same way as Murata et al. (2014).

Infrared luminosity, LIR, integrated over $8 \mu\text{m}$ to $1000 \mu\text{m}$, was estimated with the $24 \mu\text{m}$ to $500 \mu\text{m}$ photometry. We did not use the L15 photometry because it was used to derive $L8$ and to avoid any dependency between $L8$ and LIR. An SED library of Chary & Elbaz (2001) was used for the calculation. For a total of 122 galaxies LIR was derived, among which 30 have *Herschel* photometry. Although for most of galaxies the LIR were derived with only the $24 \mu\text{m}$ luminosity, they can be reliable since Elbaz et al. (2010) show infrared luminosity derived from only $24 \mu\text{m}$ band agrees with that from $24 \mu\text{m}$ and $100-500$

μm bands within 0.15 dex for galaxies at $z < 1.5$. The LIR distribution in our sample has a peak at $\log \text{LIR} \sim 11.2$, similar to the NEP-Deep field at the same redshift range.

Stellar mass, M_* , was derived with $VRi'z'$, [3.6] and [4.5] photometry using an SED library of BC03 (Bruzual & Charlot 2003). Since these six bands bracket 4000 \AA breaks, M_* can be reliably determined. We adopted SEDs of solar metallicity with $\tau = 0.1-10$ Gyr and an extinction law of Calzetti et al. (2000). We note again that the libraries used for stellar mass, photometric redshift, and infrared luminosity are different, because stellar mass estimation need more parameters than photometric redshift estimation and because dominant components for stellar mass and infrared luminosity are different so that they should be independently determined. To check whether we can see the star-formation main sequence, we plot the star-formation rate, which is the infrared luminosity multiplied by $1.09 \times 10^{-10} [\text{SFR}/L_\odot]$, and the stellar mass in Fig. 3. The star-formation main-sequence at $z = 0.6-0.85$ from Rodighiero et al. (2010) is also shown, where the difference of the initial mass function was corrected. We can see that both galaxies at $R < 2$ Mpc (red squares) and at $R > 2$ Mpc (green crosses) are on the same relation. Some galaxies are above and below the main-sequence range. Hereafter we call these galaxies galaxies above and below main-sequence.

$L8$ was derived with less uncertainty from K -correction using the L15 flux. This is because the $8 \mu\text{m}$ band is redshifted into the L15 band at $z \sim 0.8$. The K -correction was estimated with 25 SED templates from Polletta et al. (2006, 2007). The typical value of the K -correction is only ~ 0.2 dex. The IRAC4 band was used for the $8 \mu\text{m}$ band for the K -correction. Nearly 80% of our sample have $\log L8/L_\odot > 10.3$. We note that, although the L15 band almost matches the rest frame IRAC4 band, a fraction of silicate absorption at $9.7 \mu\text{m}$ could affect the $L8$ luminosity. Although this effect should be corrected by the K -correction for most of our sample, we estimated how $L8$ is affected in the worst case. We used an Arp220 template, which shows a very strong silicate absorption, and artificially masked the silicate feature to compare the L15 flux with and without the silicate feature. We confirm that 0.2 dex of the L15 flux can be reduced by the silicate absorption. However, even in the worst case, decrease of $L8$ in our results (~ 0.4 dex) cannot be explained by the silicate feature and the comparison with previous studies that derive $L8$ with similar methods is reliable.

3. Results

Previous studies suggest that when only star-forming galaxies are considered, the local environment does not affect galaxy properties. Our purpose is to extend the previous studies and to investigate whether $L8$, which is dominated by PAH emission, is dependent on the environment. To measure the $L8$ with less uncertainty of K -correction, we used the L15 band photometry. Here we provide, in section 3.1, the location (i.e. the environment) and the optical colour of galaxies to know the properties of galaxies detected with the L15 band in detail. The location of starburst galaxies with respect to the cluster core is shown in section 3.2. Then, in section 3.3, we investigate the $L8/\text{LIR}$ behaviour and compare it with those of field galaxies.

3.1. Colour and location of infrared galaxies

At $z \sim 0.8$, Koyama et al. (2008) reported that few star-forming galaxies are detected in cluster cores, and tend to be located in the medium-density region, at which optical colour shows a dra-

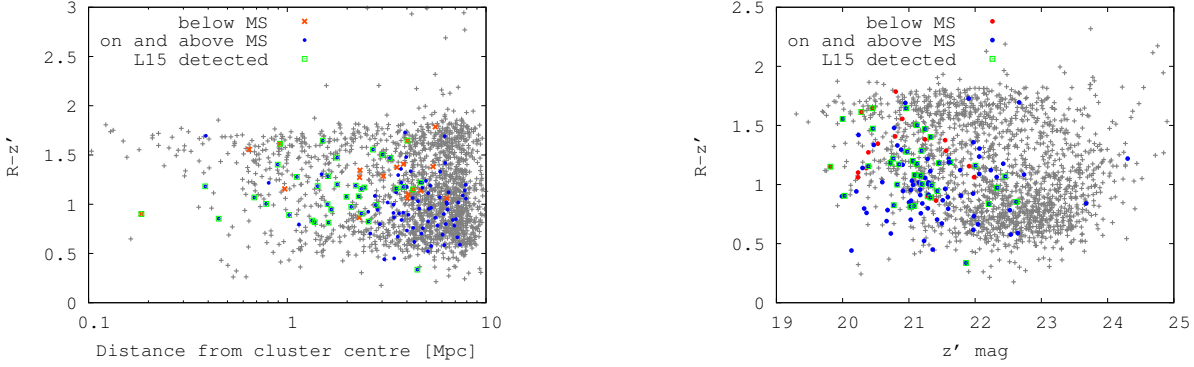


Fig. 4. Left: $R - z'$ colour vs distance from the cluster centre. The red crosses and the blue circles indicate below and on/above main-sequence galaxies, classified in Fig.3. L15 detected galaxies are indicated by the green squares. MIPS24 non-detected galaxies are also plotted with the grey points. Right: $R - z'$ vs z' colour-magnitude diagram. The symbols are the same as the left panel.

matic change. They also show that some $15\mu\text{m}$ detected galaxies in RXJ1716.4+6708, a galaxy cluster at $z = 0.81$, have optically red colours with $R - z' \geq 1.5$, which are candidates of dusty red galaxies. Marcillac et al. (2007) show that the $24\mu\text{m}$ detected galaxies in the RXJ0152, the same cluster as this study, tend to lie in the outskirts, and that they have similar colours to the late type member galaxies without $24\mu\text{m}$ detection. In our study, we show optical colours of on/above and below the main-sequence galaxies, compared with those of infrared undetected galaxies in the RXJ0152.

The left panel of Fig.4 shows the $R - z'$ colour against distance from the cluster centre. Most of the galaxies in the $R < 1$ Mpc region have red $R - z'$ colour while outer galaxies show a bimodal colour distribution, consistent with Patel et al. (2009b). On the other hand, few IR galaxies are located in $R < 1$ Mpc and a fraction of IR galaxies located at $R \sim 1$ Mpc, which is consistent with Marcillac et al. (2007). The galaxies at $R \sim 1$ Mpc show a green colour, $R - z' \sim 1.2$. Considering this region is 2-3 times denser than the average so that inter mediate density region, calculated with 5th neighbour galaxies, it is consistent with previous studies. Galaxies below the main-sequence (red crosses) has redder colour than galaxies on/above the main-sequence (blue circles). Galaxies on and above the main-sequence are merged in Fig.4 for simplicity. The average colour of below, on and above galaxies are $R - z' = 1.20 \pm 0.05$, 1.04 ± 0.03 , and 0.94 ± 0.05 , respectively. Considering dusty star-formation is strongest in galaxies above the main-sequence and weakest in galaxies below the main-sequence, the above results indicate that the optical colours are more sensitive to the star-forming activity than the dust extinction. IR galaxies at $R > 3$ Mpc seem to have bluer colour than those at $R \sim 1$ Mpc, which is consistent with Patel et al. (2009a) who show that the sSFR derived from the MIPS $24\mu\text{m}$ band decreases with increasing local density. We visually checked the 2 dimension image that these galaxies were randomly distributed so that they are not likely affected by a special clump or any instrumental error.

The right panel of Fig.4 shows the $R - z'$ versus z' colour magnitude diagram for below and on/above the main-sequence galaxies, L15 detected and IR undetected galaxies. The L15-detected galaxies show, again, a green colour, which is consistent with Koyama et al. (2008). Most of L15-detected galaxies are brighter than $z' = 22$ mag, due to the detection limits. Some L15-detected galaxies show a red colour, $R - z' > 1.5$, which is also consistent with Koyama et al. (2008). Although the L15-detected galaxies seem to be redder than other IR galaxies, it is

a selection effect due to the limited coverage of the L15 image (see Fig.1) as can be seen in the left panel of Fig.4.

3.2. Location of starburst galaxies

Here we investigate the location of starburst galaxies with respect to the cluster cores. In Fig.5, the galaxies are divided with $L8/LIR$. Galaxies with $\log L8/LIR < -0.75$, which corresponds to 1σ smaller than that of main-sequence galaxies (Elbaz et al. 2011), are regarded as starburst galaxies. The green circles in Fig.5 indicate the three clumps where above 3σ X-ray emission is encompassed (Demarco et al. 2005). We note that the $R > 2$ Mpc region is covered only partially with the L15 image (see Fig.1).

We can see that few galaxies are located in the clump, consistent with previous studies, who show a lack of star-forming galaxies in the cluster centre and X-ray clumps (Homeier et al. 2005; Marcillac et al. 2007). Fig.5 also shows that low $L8/LIR$ galaxies tend to be located in the outskirts of the cluster. As Ferré-Mateu et al. (2014) discuss that galaxies in the outskirts show a variety of star formation histories, our sample also shows that both low and high $L8/LIR$ galaxies reside in the outskirts. This can also be seen in Fig.6. In the left panel, the $L8/LIR$ is plotted against the distance from the cluster centre. We have to note that the error bars only indicate the $L8$ uncertainty. Galaxies below, on, and above the main-sequence are indicated with the green, red, and blue points for a comparison. The average and the 1σ range of the $L8/LIR$ for main-sequence galaxies in Elbaz et al. (2011) are indicated with grey lines. We can see that galaxies with $\log L8/LIR < -0.75$ are only seen at $R > 1$ Mpc regions, while higher $L8/LIR$ galaxies are located in the entire field. Similarly, we show in the right panel that galaxies with $\log \text{sSFR}/\text{sSFR}_{\text{MS}}$ above the 0.3 dex scatter (see Fig.3) are located only at $R > 1$ Mpc. These results imply that galaxies in a cluster core at $z \sim 0.8$ are not in a starburst mode.

3.3. Behaviour of $L8/LIR$ against LIR and LIR/M_*

Previous studies for field galaxies show $L8$ correlate with LIR at lower sSFR, but have a relative weakness of $L8$ at higher sSFR, throughout a redshift range of $z=0.3-2$ (Elbaz et al. 2011; Nordon et al. 2012; Murata et al. 2014). In our study, we investigate whether the $L8/LIR$ behaviour of cluster galaxies is different from those of the field galaxies using the *AKARI* L15 photometry. Our results are compared with those of *AKARI* NEP-Deep

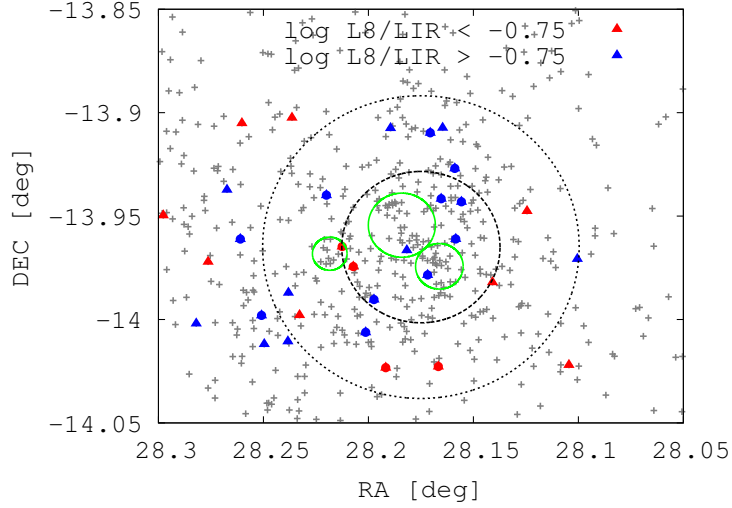


Fig. 5. Location of L15 detected galaxies. The circles and the triangles indicate galaxies with and without a spectroscopic redshift, respectively. The red and blue symbols indicate those with $\log L8/LIR < -0.75$ and $\log L8/LIR > -0.75$, respectively. This boundary corresponds to 1σ smaller than that of main-sequence galaxies determined in Elbaz et al. (2011). The grey crosses indicate the member galaxies without L15 detection. The Black dotted lines indicate the 1 and 2 Mpc radii from the cluster centre. The green solid lines indicate the three clumps in Demarco et al. (2005).

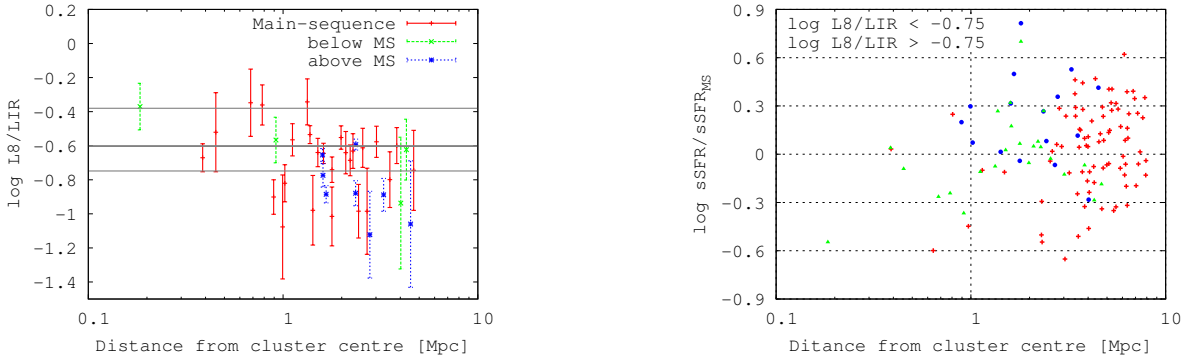


Fig. 6. Left: $L8/LIR$ vs distance from the cluster centre. The green, red, and blue points indicate the below, on, and above main-sequence galaxies in Fig.3. The grey lines indicate the average and the range of $L8/LIR$ for main-sequence galaxies in Elbaz et al. (2011). Right: $sSFR$ divided by that of main-sequence from Rodighiero et al. (2010). The blue circles and the green triangles indicate galaxies with $\log L8/LIR < -0.75$ and > -0.75 . The red crosses indicates galaxies without L15 band detection.

field studied in Murata et al. (2014), who applied similar methods to our work. We re-calculated their result from the same data set to match the redshift range with the current sample, $z_{phot} = 0.76-0.925$.

Fig.7 shows the results. The left panel shows a relation between $L8/LIR$ and $sSFR$ normalised by that of main-sequence galaxies. We applied the $sSFR$ of main-sequence galaxies from Rodighiero et al. (2010) in Fig.3. The green line indicates the average value of each point in 0.5 dex size bins, and the errors were calculated with the standard deviation divided by the square root of the number of galaxies in each bin. The $L8/LIR$ monotonically decreases with $sSFR/sSFR_{MS}$. Our result is consistent with that from the NEP-Deep field within the errors. We note that the redshift range of the main-sequence of Rodighiero et al. (2010) is different from ours, which can shift the $sSFR/sSFR_{MS}$ for both the NEP-Deep results and ours, but our conclusion does not change.

The right panel shows a relation between $L8/LIR$ and LIR . The $L8/LIR$ again monotonically decreases with LIR . The results from Chary & Elbaz (2001) at $z = 0$ and Nordon et al.

(2012) at $z = 1$ and $z = 2$ are also shown, which show the redshift evolution of the relation between $L8/LIR$ and LIR . Our result is consistent with that of the NEP-Deep field. Although the slope of the both results is slightly different from the relation from Nordon et al. (2012), they are between the relations at $z = 0$ and $z = 2$. At $\log LIR < 11.2$, however, the NEP results and ours are above the relation at $z = 2$ in Nordon et al. (2012). This is due to the $L8$ limits, as shown the black solid line in Fig.7, which leads a lack of low $L8/LIR$ galaxies at lower LIR . Hence, at lower luminosity our result can only be compared with the NEP results, whose completeness is similar to our cluster sample. The results of Fig.7 indicate that environment dependence of the redshift evolution of this relation is not remarkable. Despite limited sample, all above results support an idea that the behaviour of the $L8/LIR$ of cluster galaxies is unaffected by the environment.

4. Discussion and Conclusion

In this paper, we investigated the behaviour of $L8/LIR$ of galaxies in RXJ0152. Most notably, our study focuses on the $L8/LIR$

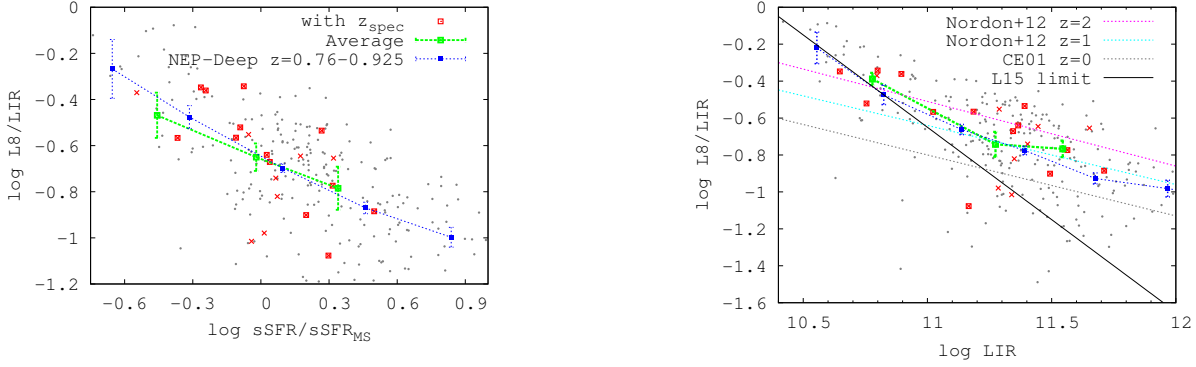


Fig. 7. Left: $L8/LIR$ vs $sSFR$ divided by that of the main-sequence of the RXJ0152 member galaxies (red crosses) compared with those of the NEP-Deep field galaxies (grey circles). The red squares indicate spectroscopically confirmed member galaxies, while red crosses indicate the member galaxies without spectroscopic redshift. The green broken line indicates the average of the red points in 0.5 dex bins, where errors are calculated with standard deviation divided by the square root of the number of galaxies in each bin. The blue dotted line indicates the average from the NEP-Deep field. The redshift range of the NEP-Deep field galaxies is restricted to $z=0.76-0.925$. Right: Relation between $L8/LIR$ and LIR . Symbols are the same as the left panel. The grey, cyan, and magenta dotted lines indicate the results from Chary & Elbaz (2001) at $z=0$ and Nordon et al. (2012) at $z=1$ and $z=2$, respectively.

behaviour, of which the measurement is difficult without using *AKARI*. We found that few galaxies in the cluster cores are detected with the L15 band and that galaxies with $\log L8/LIR < -0.75$ are located only at the outskirts of the cluster. These results are consistent with previous studies, who found the lack of star-forming galaxies in the cluster core (Homeier et al. 2005). We compared the $L8/LIR$ behaviour of the member galaxies with those of field galaxies, obtained from the AKARI NEP-Deep survey, and did not find a clear environmental dependence of the $L8/LIR$ behaviour. The average of $L8/LIR$ of both the cluster members and field galaxies decreases with $sSFR/sSFR_{MS}$ and LIR . These findings extend previous studies, supporting the idea that the relation between physical parameters of star-forming galaxies is not affected by the environments whereas the fraction of galaxy type is different in different environments.

This idea can be interpreted as that galaxies affected by the environment rapidly evolve into passive galaxies. Some researches support this interpretation. Nantais et al. (2013) found that cluster galaxies with peculiar morphology directly evolve into an early type galaxy without having a chance to first evolve into a normal spiral galaxy. Ferré-Mateu et al. (2014) show that galaxies in the cores have formed the bulk of the stars in a short period starburst at earlier epoch while galaxies in the outskirts have various star-formation histories. On the other hand, Lidman et al. (2013) show the importance of galaxy mergers for build up of the stellar mass in brightest cluster galaxies, which are not detected with our L15 band. From these studies, it is implied that galaxies in the cores have experienced a merger, evolved into passive galaxies, and are not detected with the L15 band.

However, we have some limitations to conclude the above scenario. Most of our sample galaxies are located in the outskirts of the cluster, so that the sample size of the cluster core is small. Furthermore, it is not clear whether the above scenario can apply to other cluster galaxies. Future works should therefore increase the sample size and include galaxies located in cluster cores, by using other galaxy clusters.

Acknowledgements. This research is based on observations with AKARI, a JAXA project with the participation of ESA. K.Murata is supported by JSPS (No.0263507). This work was financially supported in part by a Grant-in-Aid for the Scientific Research (No.26800107).

References

- Arnouts, S., Walcher, C. J., Le Fèvre, O., et al. 2007, *A&A*, 476, 137
- Bertin, E. & Arnouts, S. 1996, *A&AS*, 117, 393
- Blakeslee, J. P., Holden, B. P., Franx, M., et al. 2006, *ApJ*, 644, 30
- Bruzual, G. & Charlot, S. 2003, *MNRAS*, 344, 1000
- Calzetti, D., Armus, L., Bohlin, R. C., et al. 2000, *ApJ*, 533, 682
- Chabrier, G. 2003, *PASP*, 115, 763
- Chary, R. & Elbaz, D. 2001, *ApJ*, 556, 562
- Cooper, M. C., Newman, J. A., Weiner, B. J., et al. 2008, *MNRAS*, 383, 1058
- Demarco, R., Gobat, R., Rosati, P., et al. 2010, *ApJ*, 725, 1252
- Demarco, R., Rosati, P., Lidman, C., et al. 2005, *A&A*, 432, 381
- Draine, B. T. & Li, A. 2007, *ApJ*, 657, 810
- Dressler, A. 1980, *ApJ*, 236, 351
- Elbaz, D., Daddi, E., Le Borgne, D., et al. 2007, *A&A*, 468, 33
- Elbaz, D., Dickinson, M., Hwang, H. S., et al. 2011, *A&A*, 533, A119
- Elbaz, D., Hwang, H. S., Magnelli, B., et al. 2010, *A&A*, 518, L29
- Ferré-Mateu, A., Sánchez-Blázquez, P., Vazdekis, A., & de la Rosa, I. G. 2014, *ApJ*, 797, 136
- Girardi, M., Demarco, R., Rosati, P., & Borgani, S. 2005, *A&A*, 442, 29
- Homeier, N. L., Demarco, R., Rosati, P., et al. 2005, *ApJ*, 621, 651
- Ilbert, O., Arnouts, S., McCracken, H. J., et al. 2006, *A&A*, 457, 841
- Jørgensen, I., Bergmann, M., Davies, R., et al. 2005, *AJ*, 129, 1249
- Kodama, T., Tanaka, M., Tamura, T., et al. 2005, *PASJ*, 57, 309
- Koyama, Y., Kodama, T., Nakata, F., Shimasaku, K., & Okamura, S. 2011, *ApJ*, 734, 66
- Koyama, Y., Kodama, T., Shimasaku, K., et al. 2008, *MNRAS*, 391, 1758
- Koyama, Y., Kodama, T., Tadaki, K.-i., et al. 2014, *ApJ*, 789, 18
- Koyama, Y., Smail, I., Kurk, J., et al. 2013, *MNRAS*, 434, 423
- Lidman, C., Iacobuta, G., Bauer, A. E., et al. 2013, *MNRAS*, 433, 825
- Lutz, D., Poglitsch, A., Altieri, B., et al. 2011, *A&A*, 532, A90
- Marcillac, D., Rigby, J. R., Rieke, G. H., & Kelly, D. M. 2007, *ApJ*, 654, 825
- Martel, A. R., Menanteau, F., Tozzi, P., Ford, H. C., & Infante, L. 2007, *ApJS*, 168, 19
- Matsuhara, H., Wada, T., Matsura, S., et al. 2006, *PASJ*, 58, 673
- Maughan, B. J., Ellis, S. C., Jones, L. R., et al. 2006, *ApJ*, 640, 219
- Murakami, H., Baba, H., Barthel, P., et al. 2007, *PASJ*, 59, 369
- Murata, K., Matsuhara, H., Inami, H., et al. 2014, *A&A*, 566, A136
- Murata, K., Matsuhara, H., Wada, T., et al. 2013, *A&A*, 559, A132
- Muzzin, A., Wilson, G., Yee, H. K. C., et al. 2012, *ApJ*, 746, 188
- Nantais, J. B., Flores, H., Demarco, R., et al. 2013, *A&A*, 555, A5
- Nordon, R., Lutz, D., Genzel, R., et al. 2012, *ApJ*, 745, 182
- Oliver, S. J., Bock, J., Altieri, B., et al. 2012, *MNRAS*, 424, 1614
- Onaka, T., Matsuhara, H., Wada, T., et al. 2007, *PASJ*, 59, 401
- Patel, S. G., Holden, B. P., Kelson, D. D., Illingworth, G. D., & Franx, M. 2009a, *ApJ*, 705, L67
- Patel, S. G., Kelson, D. D., Holden, B. P., et al. 2009b, *ApJ*, 694, 1349
- Polletta, M., Tajer, M., Maraschi, L., et al. 2007, *ApJ*, 663, 81
- Polletta, M. d. C., Wilkes, B. J., Siana, B., et al. 2006, *ApJ*, 642, 673
- Quadri, R. F., Williams, R. J., Franx, M., & Hildebrandt, H. 2012, *ApJ*, 744, 88

- Rodighiero, G., Cimatti, A., Gruppioni, C., et al. 2010, *A&A*, 518, L25
Romer, A. K., Nichol, R. C., Holden, B. P., et al. 2000, *ApJS*, 126, 209
Rosati, P., Della Ceca, R., Norman, C., & Giacconi, R. 1998, *ApJ*, 492, L21
Stott, J. P., Collins, C. A., Sahlén, M., et al. 2010, *ApJ*, 718, 23
Takagi, T., Ohyama, Y., Goto, T., et al. 2010, *A&A*, 514, A5
Tanaka, M., Kodama, T., Arimoto, N., et al. 2005, *MNRAS*, 362, 268
Tanaka, M., Kodama, T., Arimoto, N., & Tanaka, I. 2006, *MNRAS*, 365, 1392
Tran, K.-V. H., Saintonge, A., Moustakas, J., et al. 2009, *ApJ*, 705, 809
Wada, T., Matsuhara, H., Oyabu, S., et al. 2008, *PASJ*, 60, 517
Werner, M. W., Roellig, T. L., Low, F. J., et al. 2004, *ApJS*, 154, 1